WELLBORE STABILITY ANALYSIS IN CHEMICALLY ACTIVE SHALE FORMATIONS

by

Xiang-Chao SHI*, Xu YANG, Ying-Feng MENG, and Gao LI

State Key Laboratory of Oil and Gas Reservoir Geology and Exploitation,
Southwest Petroleum University, Chengdu, China

Original scientific paper
DOI: 10.2298/TSCI16S3911S

Maintaining wellbore stability involves significant challenges when drilling in low-permeability reactive shale formations. In the present study, a non-linear thermo-chemo-poroelastic model is provided to investigate the effect of chemical, thermal, and hydraulic gradients on pore pressure and stress distributions near the wellbores. The analysis indicates that when the solute concentration of the drilling mud is higher than that of the formation fluid, the pore pressure and the effective radial and tangential stresses decrease, and v. v. Cooling of the lower salinity formation decreases the pore pressure, radial and tangential stresses. Hole enlargement is the combined effect of shear and tensile failure when drilling in high-temperature shale formations. The shear and tensile damage indexes reveal that hole enlargement occurs in the vicinity of the wellbore at an early stage of drilling. This study also demonstrates that shale wellbore stability exhibits a time-delay effect due to changes in the pore pressure and stress. The delay time computed with consideration of the strength degradation is far less than that without strength degradation.

Key words: *thermo-chemo-poroelasticity, pore pressure, time-delay effect, wellbore stability, shale*

Introduction

Filtrate invasion into shale formations causes large changes in the pore pressure, temperature, stress, and rock strength, which in turn affect the shale wellbore stability. It is well known that fluid movement from the wellbore to low-permeability shale formations is primarily controlled by osmosis effects [1-3]. Many researches have shown that the effect of water flow due to chemical and thermal gradients can sometimes be several times higher than the effect of hydraulic gradients, particularly when drilling in high-temperature and high-pressure environments [4-9]. Heidug *et al.* [4] developed the first fully coupled chemo-hydro-mechanical model to consider hydration swelling of water-active rocks. Ghassemi *et al.* [6] presented a coupled chemo-poroelastic model for hydration swelling of shale under linear conditions. Ghassemi *et al.* [7] and Zhou *et al.* [8] extended the coupled model [6] and investigated the influence of chemical osmosis and thermal osmosis on pore pressure and stress distribution in swelling shale formations. Roshan *et al.* [9] extended the work of Ghassemi *et al.* [7] by providing a coupled chemo-poroelastic model describing the evolution of pore pressure and stresses around a wellbore in relatively highly permeable shale. Later, Roshan *et al.* [10] investigated the effects of

* Corresponding author; e-mail: sxcdream@163.com

thermo-poroelastoplasticity on stresses around a wellbore in swelling shale formations. Wang *et al.* [11] built a fluid-solid-chemistry coupling model considering the effect of electrochemical potential osmosis, solute diffusion, and ion transmission. Shen *et al.* [12] presented a coupled poro-thermo-elastic model in a saturated linear medium and discussed the cooling-induced pore pressure and stress distribution along the radial direction.

In the mentioned studies, the mechanical properties of swelling shale are considered as constant. Previous studies indicate that the long-term strength decrease with time is due to the effect of the rheology of shale [13-15]. In this study, a non-linear thermo-chemo-poroelastic model is developed and the distribution of pore pressure and stress around a wellbore is presented. Then, the shale wellbore stability, considering the effect of filtrate invasion on the time-dependent variation of shale strength, is presented and discussed.

Non-linear thermo-chemo-poroelastic model

Low-permeability reactive shale is considered a linearly elastic material. It is assumed that shale swells or shrinks in response to variation of the chemical potential and temperature. The total stress is defined [7, 9]:

$$\dot{\sigma}_{ij} = 2G\dot{\varepsilon}_{ij} + \left(K - \frac{2}{3}G\right)\dot{\varepsilon}_{kk}\delta_{ij} - \alpha_{\mathrm{B}}\dot{p}\delta_{ij} - K\alpha_{\mathrm{s}}\dot{T}\delta_{ij} + \omega_0\frac{M_{\mathrm{s}}}{\mathrm{R}T}(\dot{\mu}_{\mathrm{s}} + \dot{\mu}_{\mathrm{d}})\delta_{ij} \tag{1}$$

where σ_{ij} and ε_{ij} are components of the total stress tensor and total strain tensor, respectively, p – the pore pressure, K and G are bulk and shear moduli, respectively, α_{B} – the Biot coefficient, T – the temperature, α_{s} – the thermal expansion coefficient of a solid skeleton, ω_0 – the chemical swelling coefficient, M_{s} – the molar mass of the solute, R – the universal gas constant, μ_{s} and μ_{d} are the chemical potential of the solute and diluent, respectively, and δ_{ij} – the Kronecker delta.

The variation of the fluid content is as follows [7]:

$$\dot{e} = \alpha_{\mathrm{B}}\dot{\varepsilon}_{ii} + \frac{\alpha_{\mathrm{B}} - \phi}{K_{\mathrm{s}}}\dot{p} - \gamma\dot{T} + \omega_0\frac{M_{\mathrm{s}}}{\mathrm{R}T}\frac{\alpha_{\mathrm{B}} - 1}{K}(\dot{\mu}_{\mathrm{s}} + \dot{\mu}_{\mathrm{d}}) \tag{2}$$

where α_{B} and γ are given by:

$$\alpha_{\mathrm{B}} = 1 - \frac{K}{K_{\mathrm{s}}} = \frac{3(\nu_{\mathrm{u}} - \nu)}{B(1 + \nu_{\mathrm{u}})(1 - 2\nu)} \tag{3}$$

$$\gamma = \alpha_{\mathrm{B}}\alpha_{\mathrm{s}} + (\alpha_{\mathrm{f}} - \alpha_{\mathrm{s}})\phi \tag{4}$$

where ν is the drained Poisson's ratio, ν_{u} – the undrained Poisson's ratio, B – the Skempton's coefficient, ϕ – the porosity, K_{s} – the solid bulk modulus, and α_{f} – the thermal expansion coefficient of fluid.

It is assumed that fluid flow is governed by hydraulic flow, thermal osmosis, and chemo osmosis. Solute flux is due to diffusion and thermal filtration. Heat transfer obeys Fourier's law; hence:

$$J_{\mathrm{f}} = -\rho_{\mathrm{f}}\frac{k}{\mu}\left(\nabla p - \frac{\lambda\rho_{\mathrm{f}}\mathrm{R}T}{C_{\mathrm{s}}C_{\mathrm{d}}M_{\mathrm{s}}}\nabla C_{\mathrm{s}}\right) + \rho_{\mathrm{f}}K_{\mathrm{T}}\nabla T \tag{5}$$

$$J_{\mathrm{s}} = -\rho_{\mathrm{f}}D_{\mathrm{s}}\nabla C_{\mathrm{s}} - \rho_{\mathrm{f}}D_{\mathrm{T}}\nabla T \tag{6}$$

$$J_{\mathrm{T}} = -K_{\mathrm{T}}\nabla T \tag{7}$$

where ρ_f is the fluid mass density, k – the permeability, μ – the fluid viscosity, C_s – the solute fraction, C_d – the diluent fraction, λ – the reflection coefficient, K_T – the thermal osmosis coefficient, D_s – the solute diffusion coefficient, and D_T – the solute thermal diffusion coefficient.

Substituting these constitutive equations into balance equations of force and continuity, one can obtain the following field equations:

$$\left(K+\frac{G}{3}\right)\nabla(\nabla u)+G\nabla^2 u+\left(\alpha_B-\frac{\omega_0 M_s}{C_d\rho_f RT}\right)\nabla p+K\alpha_s\nabla T-\omega_0\left(\frac{1}{C_s}-\frac{1}{C_d}\right)\nabla C_s+f_i=0 \quad (8)$$

$$\alpha_B\dot{\varepsilon}_{ii}+\left(\frac{\alpha_B-\phi}{K_s}+\frac{\phi}{K_f}+\frac{\omega_0 M_s}{C_d\rho_f RT}\frac{\alpha_B-1}{K}\right)\dot{p}-\gamma\dot{T}+\omega_0\frac{\alpha_B-1}{K}\left(\frac{1}{C_s}-\frac{1}{C_d}\right)\dot{C}_s=$$

$$=\nabla\left[\frac{k}{\mu}\left(\nabla p-\frac{\lambda\rho_f RT}{C_s C_d M_s}\nabla C_s\right)\right]-K_T\nabla^2 T \quad (9)$$

$$\phi\dot{C}_s-D_s\nabla^2 C_s-C_s D_T\nabla^2 T=0 \quad (10)$$

$$\dot{T}+u_f\nabla T-c_T\nabla^2 T=0 \quad (11)$$

where u is the displacement, f_i – the body force, u_f – the fluid velocity, and c_T – the thermal diffusivity coefficient.

Pore pressure distribution

The coupled non-linear eqs. (8)-(11) were solved using COMSOL multiphysics software. The computational grid is shown in fig. 1. Note that a quarter of the drilling well with a wellbore radius (r_m) of 0.1 m is discretized considering the effect of symmetry. When the solute concentration of the drilling mud is lower than that of the formation fluid ($C_m < C_{sh}$), $C_m = 0.1$ and $C_{sh} = 0.2$. However, for cases with higher salinity of the drilling mud, $C_m = 0.2$ and $C_{sh} = 0.1$. The initial temperature of shale formation T_{sh} is 375 K. For cooling cases ($T_m < T_{sh}$), the temperature of the drilling mud is set to 325 K. The distribution of the pore pressure is presented in fig. 2. It can be seen from the figure that the pore pressure increases with lower salinity drilling mud, while it decreases for higher salinity drilling mud. When the tempera-

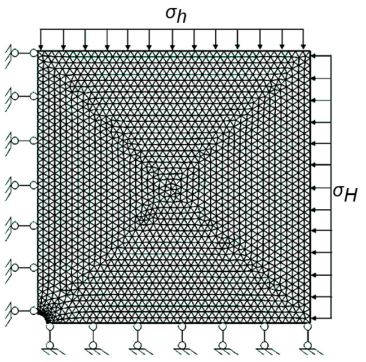

Figure 1. Computational grid

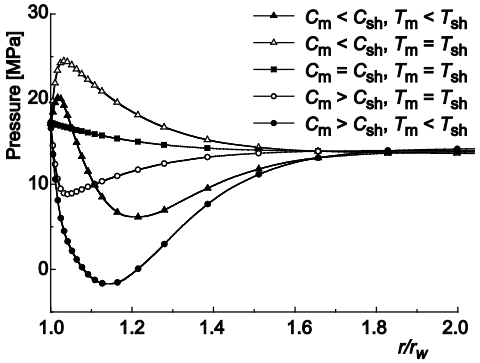

Figure 2. Pore pressure distribution along *y*-axis

ture of drilling mud is lower than that of formation ($T_m < T_{sh}$), the decrement of the pore pressure is more obvious.

Here, we compare the results of the linear model and non-linear model when the wellbore wall is suddenly cooled. Figure 3 presents the distribution of the pore pressure for the cases of $C_m < C_{sh}$ and $C_m > C_{sh}$ at different time steps. It is found that the pore pressure calculated by the non-linear model is higher than that for the linear model. This is particularly evident in the case of $C_m < C_{sh}$. The accuracy of the pore pressures obtained from the linear and non-linear model may be acceptable when the difference between C_m and C_{sh} is relatively small under isothermal conditions [8]. It is obvious that when the difference between the temperature of the drilling mud and the formation is relatively large, the linear model tends to underestimate the pore pressures.

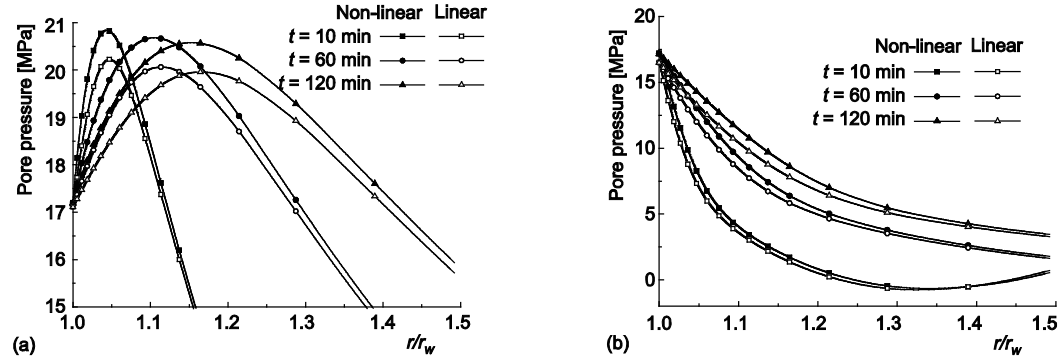

Figure 3. Distribution of pore pressure along *y*-axis for (a) $C_m < C_{sh}$ and (b) $C_m > C_{sh}$

Wellbore stability analysis

The Mohr-Coulomb failure criterion is used to determine the progress of damage under shear stress:

$$f_c = -\sigma_1' + \sigma_3' \frac{1+\sin\varphi}{1-\sin\varphi} + \frac{2c\cos\varphi}{1-\sin\varphi} \tag{12}$$

where σ_1' and σ_3' are the maximum and minimum effective principle stresses, respectively, c – the cohesion, and φ – the friction angle.

When the effective radial stress near the wellbore reaches the limit of tensile strength, the exfoliation mode of failure will be encountered:

$$f_1 = \sigma_3' + s_t \tag{12}$$

where s_t is the tensile strength.

The distributions of the effective radial and tangential stresses along the *y*-axis for different combinations of the boundary conditions are presented in fig. 4. When the solute concentration of the drilling mud is higher than that of the formation fluid, both the effective radial and tangential stresses near the wellbore decrease, and *v. v.* Cooling of the formation decreases both the effective radial and tangential stresses. For example, the effective radial stress near the wellbore region when $C_m > C_{sh}$ and $T_m < T_{sh}$ is −4.97 MPa. This may lead to an exfoliation mode of failure near the wellbore. However, the effective radial stress for the wellbore wall remains the same.

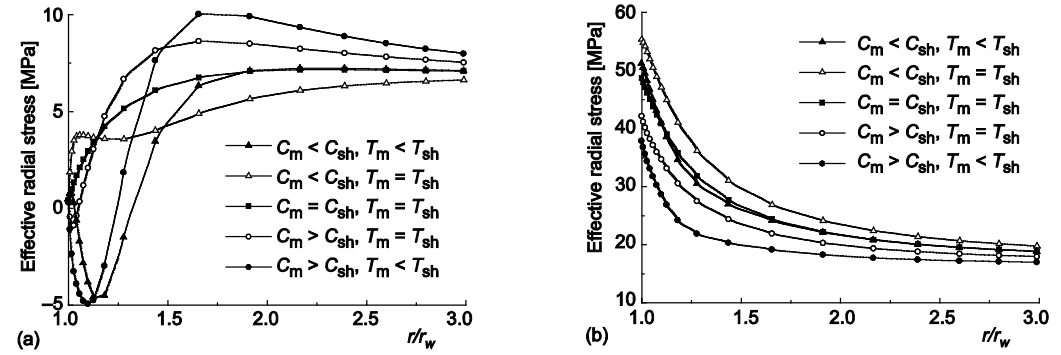

Figure 4. Distribution of effective stress along *y*-axis at 100 seconds for (a) radial and (b) tangential

Figure 5 illustrates the evolution of the shear failure around the wellbore for cooling ($T_m < T_{sh}$) for two different cases: $C_m < C_{sh}$ and $C_m > C_{sh}$. It should be noted that the strength of shale may decrease due to hydration and swelling of the clay minerals [5, 14]. However, the strength can be considered constant at an early stage of drilling. It is found that well collapse first occurs in the vicinity of the wellbore ($f_c < 0$). With time, the peak value of f_c decreases, suggesting enhanced wellbore stability with respect to shear failure.

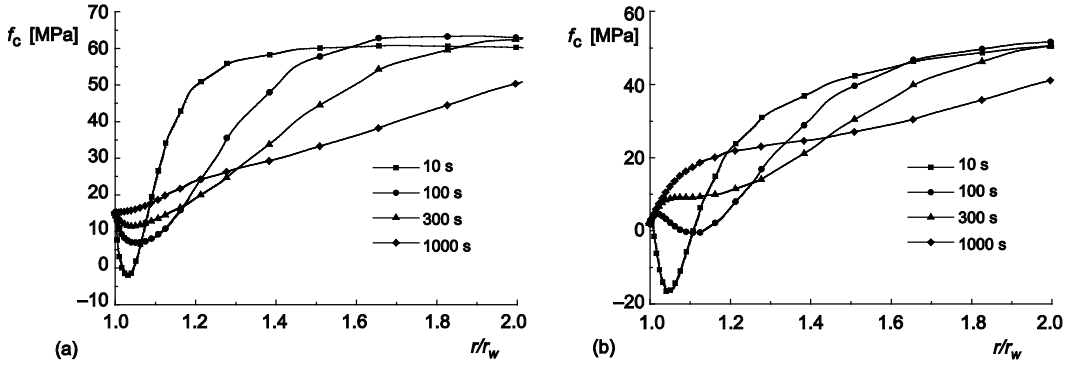

Figure 5. Evolution of shear failure along *y*-axis for (a) $C_m < C_{sh}$ and (b) $C_m > C_{sh}$

The evolution of the tensile failure along the *y*-axis for two different boundary conditions is presented in fig. 6. It can be observed that the damage index, f_l, near the wellbore is less than 0, which indicates that the exfoliation mode of failure occurs in formations near the wellbore. This is because cooling of the formation causes a large decrease in the effective radial stress, increasing the tensile stress when compared with that in isothermal condition. With time, f_l increases, suggesting enhanced wellbore stability with respect to tensile failure. Therefore, rock failure around the wellbore for high-temperature shale formations is due to a combination of shear failure and tensile failure. Their combined effect may cause hole enlargement or even lead to well collapse.

In the previous analysis, the strength of shale is considered to be constant. Several researches have shown that the strength decreases with time because of filtrate invasion [5, 14]. When porous flow is considered, the strength can be expressed as follows [13, 14]:

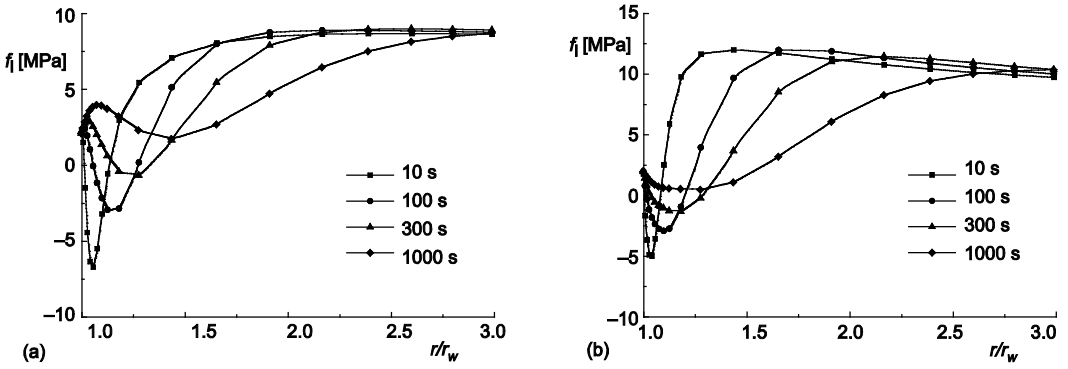

Figure 6. Evolution of tensile failure along *y*-axis for (a) $C_m < C_{sh}$ and (b) $C_m > C_{sh}$

$$c(s) = c_0 - 58.8(s - s_\infty) \tag{13}$$

$$\varphi(s) = \varphi_0 - 187.5(s - s_\infty) \tag{14}$$

where $c(s)$ and $\varphi(s)$ denote the cohesion and internal friction angle, respectively, c_0 and φ_0 denote the initial cohesion and internal friction angle, respectively, s is the instantaneous water content, and s_∞ is the initial formation water content.

The evolution of the shear failure damage index, f_c, with time at the wellbore (x = 0 m and y = 0.1 m) is shown in fig. 7. In this analysis, the solute concentration in the mud is kept higher than that of the shale formation ($C_m > C_{sh}$). At an early stage (t < 300 s), shear failure is encountered, which leads to hole enlargement. With time, f_c first increases and then decreases. The hole becomes unstable after 46.7 hours due to the strength degradation of shale. While the delay time is 86.6 hours, when the strength of shale is considered constant. There is a potential risk of wellbore instability when the instantaneous strength is considered, and the stable borehole at the start of drilling will probably collapse with time. This phenomenon is called the time-delay effect of wellbore instability. The pore pressure and stress changes near the wellbore are the main factors that contribute to the time-delay effect, and the delay time is significantly affected by the strength degradation. It should be noted that with time, a chemical and thermal equilibrium is reached, gradually causing the tensile failure to disappear. Therefore, the evolution of the damage index f_t (tensile failure) is not provided.

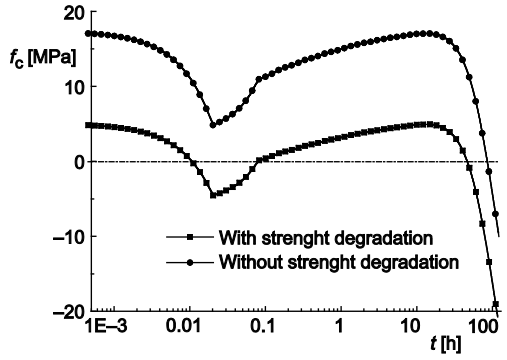

Figure 7. Evolution of shear failure damage index with time at the wellbore (x = 0 and y = 0.1)

Conclusions

A coupled non-linear thermo-chemo-poroelastic model has been used to investigate the distribution of temperature, pore pressure, and stress around a wellbore in swelling shale formations. It has been observed that when the solute concentration of the drilling mud is lower than that of the formation fluid, the filtrate tends to flux in the shale formation, increasing the pore pressure (and *v. v.*). Cooling of the formation tends to decrease the formation pore pressure.

When the salinity of the drilling mud is higher than that of the formation fluid, the effective radial and tangential stresses decrease, and *v. v.* When the temperature of the drilling mud with a higher salinity is lower than that of the formation fluid, the decrease in stress is more obvious, resulting in increased tensile stress.

Hole enlargement is the combined effect of shear and tensile failure when the high-temperature formation is suddenly cooled. Damages first occur in the vicinity of wellbore. The shear and tensile failure damage indexes increase with time, suggesting enhanced wellbore stability. Wellbore stability of swelling shale exhibits a time-delay effect due to changes in the pore pressure and stress, and the delay time is significantly influenced by the strength degradation of shale.

Acknowledgment

This work was financially supported by the Youth Foundation of National Natural Science Foundation of China (No. 51504208) and the Youth Scientific Research Foundation of Southwest Petroleum University (No. 2012XJZT003).

References

[1] Chenevert, M., *et al.*, Shale Control with Balanced-Activity Oil-Continuous Muds, *Journal of Petroleum Technology*, *22* (1970), 10, pp. 1309-1316
[2] Gomar, M., *et al.*, A Transient Fully Coupled Thermo-Poroelastic Finite Element Analysis of Wellbore Stability, *Arabian Journal of Geosciences*, *8* (2015), 6. pp. 1-11
[3] Mody, F., *et al.*, Borehole-Stability Model to Couple the Mechanics and Chemistry of Drilling-Fluid/Shale Interactions, *Journal of Petroleum Technology*, *45* (1993), 11, pp. 1093-1101
[4] Heidug, W., *et al.*, Hydration Swelling of Water-Absorbing Rocks: A Constitutive Model, *International Journal for Numerical & Analytical Methods in Geomechanics*, *20* (1996), 6, pp. 403-430
[5] Ma, T., *et al.*, A Wellbore Stability Analysis Model with Chemical-Mechanical Coupling for Shale Gas Reservoirs, *Journal of Natural Gas Science & Engineering*, *26* (2015), Sep., pp. 72-98
[6] Ghassemi, A., *et al.*, Linear Chemo-Poroelasticity for Swelling Shales: Theory and Application, *Journal of Petroleum Science & Engineering*, *38* (2003), 3, pp. 199-212
[7] Ghassemi, A., *et al.*, Influence of Coupled Chemo-Poro-Thermoelastic Processes on Pore Pressure and Stress Distributions around a Wellbore in Swelling Shale, *Journal of Petroleum Science & Engineering*, *67* (2009), 1, pp. 57-64
[8] Zhou, X., *et al.*, Finite Element Analysis of Coupled Chemo-Poro-Thermo-Mechanical Effects around a Wellbore in Swelling Shale, *International Journal of Rock Mechanics & Mining Sciences*, *46* (2009), 4, pp. 769-778
[9] Roshan, H., *et al.*, A Fully Coupled Chemo-Poroelastic Analysis of Pore Pressure and Stress Distribution around a Wellbore in Water Active Rocks, *Rock Mechanics & Rock Engineering*, *44* (2011), 2, pp. 199-210
[10] Roshan, H., *et al.*, Analysis of Pore Pressure and Stress Distribution around a Wellbore Drilled in Chemically Active Elastoplastic Formations, *Rock Mechanics & Rock Engineering*, *44* (2011), 5, pp. 541-552
[11] Wang, Q., *et al.*, A Fluid-Solid-Chemistry Coupling Model for Shale Wellbore Stability, *Petroleum Exploration & Development*, *39* (2012), 4, pp. 508-513
[12] Sheng, J., *et al.*, Analysis of Coupled Porothermoelastic Response of a Wellbore by Using a Femlab-based Simulator, *Engineering Mechanics*, *25* (2008), 2, pp. 219-223
[13] Jin, Y., *et al.*, A Method for Determining the Critical Time of Wellbore Instability at Water-Sensitive Shale Formations, *Petroleum Drilling Techniques*, *32* (2004), 2, pp. 12-14
[14] Lu, Y.. *et al.*, Influence of Porous Flow on Wellbore Stability for an Inclined Well with Weak Plane Formation, *Petroleum Science & Technology*, *31* (2013), 6, pp. 616-624
[15] Yuan, J., *et al.*, Borehole Stability Analysis of Horizontal Drilling in Shale Gas Reservoirs, *Rock Mechanics & Rock Engineering*, *46* (2013), 5, pp. 1157-1164

Paper submitted: December 14, 2015
Paper revised: December 20, 2015
Paper accepted: December 25, 2015